

Induced Ferromagnetism and Anisotropy of Pt Layers in Fe/Pt(001) Multilayers

W. J. Antel Jr., M. M. Schwickert, Tao Lin
Dept. of Physics and Astronomy, Ohio University, Athens, OH 45701

W. L. O'Brien
Synchrotron Radiation Center, University of Wisconsin-Madison, 3731 Schneider Dr., Stoughton, WI 53589

G. R. Harp
Dept. of Physics and Astronomy, Ohio University, Athens, OH 45701
(January 6, 1999)

The structural and magnetic properties of sputter deposited epitaxial Fe 7.5 Å/Pt t_{Pt} (001) multilayers ($t_{Pt} = 0-15$ Å) are investigated using x-ray diffraction, Kerr magnetometry, and x-ray magnetic circular dichroism (XMCD). X-ray diffraction shows that there is a crystalline phase change from bct to fct at a Pt thickness of ≈ 4 Å. The Fe XMCD is enhanced by $\approx 10\%$ over its bulk value for Pt thicknesses from 1-4 Å (bct region), and depressed relative to the bulk by 10-20% after transition to the fct phase. The Pt layers show a striking “almost ferromagnetic” behavior. XMCD at the $N_{2,3}$ edge shows that the Pt moment is nearly constant up to $t_{Pt} = 10$ Å, with a value of $\approx 0.5 \mu_B/\text{atom}$. Kerr magnetometry is used to determine the in plane magnetocrystalline anisotropy constant, K_1 , as a function of t_{Pt} . It is found that for the Fe thickness studied here, the easy axis switches from the bct[100] to the bct[110] direction with increasing t_{Pt} . This indicates that K_1 has a zero crossing, which occurs at $t_{Pt} \approx 1.5$ Å. This strong variation in magnetic anisotropy is attributed mainly to the Fe/Pt interface region. However, ferromagnetic Pt also contributes a significant volume anisotropy which we estimate at $-8 \pm 2 \times 10^5$ erg/cc.

PACS numbers: 75.70.-i

I. INTRODUCTION

The applications of magnetic materials for storage purposes would appear to be limitless. However each new application has more strenuous materials requirements from the one used before. To fill this need, interest in multilayered systems has increased sharply due to the flexibility that these systems present for variation in their magnetic properties. Fe/Pt multilayers have received some research attention in the recent past. The majority of this research has focused on the (111) orientation. [1]

In the current investigation, (001) Fe/Pt multilayers are studied. There have been only a few other studies on this orientation. One examined the crystal structure and anisotropy as a function of Fe thickness, t_{Fe} , while keeping the Pt thickness, t_{Pt} , constant at 13.5 Å. [2] There it was found that the Fe underwent a structural transition at $t_{Fe} \approx 8$ Å. For t_{Fe} less than this critical thickness, the Fe lattice was tetragonally distorted, with a compressed

in plane lattice spacing and expanded out of plane spacing. Greater than this thickness, both in and out of plane lattice spacings were close to that of bcc Fe.

Reference [2] studied the magnitude and sign of the perpendicular magnetic anisotropy over an Fe thickness range of $t_{Fe} = 3-34$ Å. They reported that for sufficiently thin Fe layers, net perpendicular anisotropy could be obtained. The in plane anisotropy constant, K_1 , was measured for $t_{Fe} > 8$ Å (bct Fe). They found that K_1 was nearly constant for all $t_{Fe} > 8$ Å, with a value of $\approx 4.6 \times 10^5$ erg/cc.

In another study the (001) oriented system was studied as a function of Pt thickness (bcc Fe, t_{Fe} held constant at 25.2 Å). [3] Antiferromagnetic coupling was observed between the Fe layers for $t_{Pt} = 19.4$ Å. Using bulk magnetometry, it was also found that the magnetization is constant as a function of Pt thickness, suggesting a negligibly small induced Pt moment. X-ray diffraction was performed for $t_{Pt} = 13-22$ Å, and showed a superposition of bcc (Fe) and fcc (Pt) structures in this thickness range.

The current study investigates the structural and magnetic properties as a function of Pt thickness using thin Fe layers ($t_{Fe} = 7.5$ Å). We find that for $t_{Pt} \lesssim 10$ Å (5 ML), the Pt layers are ferromagnetic with a constant Pt moment of $\approx 0.5 \mu_B$. The in plane anisotropy contribution from the Fe/Pt interface is large, due to the symmetry breaking which occurs there. Indeed, the interface anisotropy constant K_s is so large that the effective in plane magnetocrystalline anisotropy constant, K_1 , switches from positive to negative upon formation of the interface. Furthermore, the volume anisotropy constant of the ferromagnetic Pt layer appears to be negative, and we estimate its value at $-8 \pm 2 \times 10^5$ erg/cc.

As with other (001) multilayers composed of Fe and an fcc transition metal [19,20,23], the multilayers undergo a *coherent* structural phase change from bct to fct with increasing Pt layer thickness. By this we mean that both the Fe and Pt undergo the phase transition together. However, this does not strongly affect the Fe or Pt magnetic moments as is sometimes observed (see e.g. [19]). Moreover, K_1 is hardly affected by the phase change.

II. SAMPLE PREPARATION

Although several samples were prepared for preliminary measurements, this study focuses on one Fe/Pt multilayer film prepared on a 2" long MgO(001) substrate. The Pt layer thickness was varied from 0-15 Å from one side of the substrate to the other (Pt wedge) to allow thickness-dependent measurements of films prepared under identical conditions. The sample was grown in a magnetron sputter deposition system with a base pressure of 5×10^{-10} Torr, and a 3.25×10^{-3} Torr Ar atmosphere during sputtering. Before growth the substrate was polished with a 0.05μ alumina and water solution, inserted into the chamber, and then annealed at 600°C.

Crystalline growth was obtained through the use of established methods [7,8]. For the Fe/Pt multilayer, a buffer layer of 25 Å Cr was deposited at 600°C (to obtain epitaxy with the substrate), with another 300 Å Cr at 300°C (to obtain a flatter starting surface), and finally 25 Å Cr at 200°C just before growth of the multilayer. The multilayer was then deposited at 200°C and consisted of a constant Fe layer and a wedge of Pt: [7.5 Å Fe/0-15 Å Pt]₂₀. To prevent oxidation a capping layer of 20 Å Si₃N₄ was deposited.

An (001) oriented Co_xPt_y ($x=0\%-100\%$, $y=100\%-0\%$) alloy, used as a standard for the XMCD measurements, was prepared in the same chamber. This alloy was grown on a 2" long MgO(001) substrate. The preparation of the substrate prior to growth was as with the multilayer. The buffer layers consisted of the following deposited at 600°C, 4 Å Fe/15 Å Pt/100 Å CoPt. On top of these, the alloy itself was grown. The Co and Pt were deposited in a double wedge formation, the Co with a positive slope, the Pt with a negative slope. These wedges were deposited at 560°C, thus interdiffusion of the layers was high resulting in an alloy with a linear variation in Pt and Co concentrations. The structure was: [0-2.47 Å Pt/2.24-0 Å Co]₄₀₀. A capping layer of 15 Å Si₃N₄ was then deposited.

III. STRUCTURAL CHARACTERIZATION USING X-RAY DIFFRACTION

Structural characterization of the films was performed using specular and off-normal x-ray diffraction. X-ray scans were taken with a fixed-anode diffractometer with 1° angular resolution and Cu K_α radiation. In the interest of clarity, all crystallographic directions are referenced to the bct structure. Two surface normal (c -axis or [001]) radial scans are displayed on the left hand side of fig. 1. The single Fe/Pt multilayer feature (the bct(002)) is marked with an arrow in each scan, and the multilayer satellite is numbered. The multilayer features appear somewhat broadened because the finite size of the x-ray beam averages over a range of t_{Pt} of about 1 Å. Additionally, some of this broadening can be attributed to the

proportionality (given by the Scherrer formula) between peak width and crystal coherence length [9,10]. The crystal coherence length, is that length over which the atomic positions are correlated with one another. We can use this relation to obtain a lower limit on the value of the crystal coherence length. It is found that at $t_{Pt}=2.6$ Å, the c -axis crystal coherence length is ≈ 70 Å, while at $t_{Pt}=6.4$ Å the coherence length is ≈ 110 Å. In both cases, this corresponds to about 35% of the total crystal thickness.

The angle of this peak can be used to obtain an average lattice constant (LC) for the c -axis as a function of Pt thickness. The c -axis LC, extracted from such scans, is plotted versus Pt thickness in fig. 2. For the thinnest Pt layers, the LC is close to that of bcc Fe. As the Pt thickness is increased the LC approaches that of fcc Pt. For $t_{Pt} \approx 4$ Å, there is a jump and change of slope of the c -axis LC. We interpret this as evidence for a phase transition in the crystal structure from bct to fct.

To confirm this phase transition, two positions were studied in detail using off-normal radial scans (right hand side of fig. 1). Small pieces of the Fe/Pt wedge were cleaved out for this study to ensure that the Pt thickness varied by no more than 1 Å over the region illuminated by the x-ray beam. This left part of the aluminum sample holder exposed, and several Al features are present in fig. 1.

The first scan was taken at $t_{Pt} = 1.9$ Å through the Fe/Pt bct(103) peak (fig. 1). From the position of the (103) feature, the a -axis is found to be 2.81 Å. This is contracted slightly from the bulk Fe LC of 2.87 Å. The radial scan along the surface normal for this position yields a value for the c -axis of 3.01 Å (i.e. expanded relative to bulk Fe). From this we calculate the c/a ratio to be 1.07. This implies a bct lattice that is distorted from cubic by 7%, but still reasonably close to a bcc structure for which $c/a = 1$. Phi scans (not shown) through the Fe/Pt(103) and MgO(113) indicate an epitaxial relation of Fe/Pt bct[100] || MgO[110].

The second off-normal scan was taken at a position with $t_{Pt} = 6.4$ Å (see fig. 1). Note that this is beyond the critical thickness of 4 Å observed in fig. 2. The Fe/Pt bct(103) and bct(002) peaks were used to determine LC values of $a = 2.68$ Å and $c = 3.74$ Å. The ratio of c/a is therefore 1.40, comparable to $c/a = 1.41$ for a perfect fcc lattice. From this we learn the lattice is fct, with only 1% tetragonal distortion. In this scan, the MgO(113) is also evident, demonstrating an epitaxial relation of Fe/Pt bct[100] || MgO[110]. We note that if the multilayer were indexed on an fct lattice, this relationship would be expressed as Fe/Pt fcc[110] || MgO[110].

IV. MAGNETO OPTIC KERR MAGNETOMETRY

Magnetic characterization was performed using a magneto optic Kerr effect (MOKE) magnetometer. Typical

in plane easy and hard axis loops are displayed in fig. 3. Here we observe that for $t_{\text{Pt}} = 0.8 \text{ \AA}$, the bct[100] direction is easy, while for $t_{\text{Pt}} = 6.4 \text{ \AA}$ the bct[100] is a hard direction. We return to this point below. Although the Fe/Pt system has been shown to exhibit strong perpendicular anisotropy for certain values of the Fe and Pt thicknesses, [11,12] this is not the case for any of the films studied here; axial loops display high saturation fields ($>8 \text{ kOe}$, the highest field possible in our magnetometer) for all values of t_{Pt} . While we cannot rule out a weak perpendicular surface anisotropy constant in these films, our focus here is on the in plane anisotropy.

The saturation Kerr effect, Θ_K^{sat} , (which contains contributions from both the Kerr rotation and Kerr ellipticity) is plotted as a function of Pt thickness in fig. 4. It can be seen that while the multilayer remains in the bct crystal structure, there is a strong enhancement in the Kerr response over that for bulk Fe (0 \AA Pt in the figure). This is followed by a sharp reduction of Θ_K^{sat} in the region of the bct \rightarrow fct phase transition. Finally, in the fct region, Θ_K^{sat} decreases smoothly as expected from a simple dilution of the Kerr effect for increasing Pt concentration.

In all our studies of Fe/TM(001) oriented multilayers (TM = transition metal), including TM = V, Cr, Co, Ni, Nb, Mo, Ru, Rh, Pd, Ta, W, and Pt, [17,19,21,24,20,31] this is by far the strongest enhancement of the longitudinal Kerr effect we have observed. This enhancement is no doubt caused by 1) a significant induced Pt magnetic moment and 2) the large spin orbit coupling in Pt. The latter point is understood as follows. In the single electron Hamiltonian the spin orbit term can be written $H_{\text{SO}} = \xi \mathbf{L} \cdot \mathbf{S}$, where ξ is the spin orbit coupling parameter. ξ tends to increase with increasing atomic number, and $\xi_{\text{Fe}} = 0.076 \text{ eV}$, while $\xi_{\text{Pt}} = 0.6 \text{ eV}$ [13]. Furthermore, it is well known that to first order the Kerr effect depends linearly on ξ . [14] Thus the presence of spin-polarized Pt atoms in the Pt layer leads to a large enhancement of the Kerr effect.

The switching of the easy axis in the MOKE loops of fig. 3 leads us to examine the magnetic anisotropy more closely. The in plane magnetocrystalline anisotropy constant, K_1 , is determined from the MOKE loops by two methods, derived as follows. Let ϕ denote the angle between the magnetic easy axis and the applied field, \vec{H} . We assume uniform rotation of the film magnetization, \vec{M}_s , and the angle between \vec{M}_s and \vec{H} is θ . The total magnetic energy, W , is then given as a sum of the anisotropy energy per unit volume and the Zeeman energy. An expression in three-dimensions is given in Brailsford. [15] If we restrict \vec{M}_s to lie in the plane of the film we obtain: [16]

$$W = -M_s H (\sin \phi \sin \gamma + \cos \phi \cos \gamma) + \frac{K_1}{8} (1 - \cos 4\gamma) \quad (1)$$

Here $\gamma = \phi - \theta$. The magnitude of \vec{M}_s is determined using

a weighted average of the Fe and Pt magnetic moments as determined by XMCD (see section VI). Under an arbitrary applied field, the magnetization changes direction so as to minimize the magnetic energy. Minimizing equation 1 with respect to γ , we find

$$H = \frac{K_1}{2M_s} \frac{\sin 4(\phi - \theta)}{\sin \theta}. \quad (2)$$

More specifically, along the hard axis the saturation field is given by

$$H_{\text{sat}} = \frac{2K_1}{M_s} \quad (3)$$

Equation 3 suggests a simple method for determining K_1 by measuring the saturation field along the hard axis. The results of this analysis is shown in fig. 5 (circled crosses).

The analysis using equation 3 suffers from the fact that the hard axis saturation field is not always well defined (due to hysteresis). To provide a check on this analysis, K_1 was also determined using a second technique. For several Pt thicknesses, many loops were taken as a function of applied field direction (i.e. for various angles of ϕ). From each loop, the 95% saturation field, H_{95} , was extracted. Under this condition we then have $\theta = 18^\circ$. H_{95} is then plotted as a function of ϕ , and equation 2 is fit to this curve using K_1 as a fitting parameter. The K_1 values determined by the second method are plotted in fig. 5 with bowtie symbols. As can be seen, there is very close agreement between the values obtained using both methods.

In fig. 5, K_1 starts out close to the bulk anisotropy constant of Fe, which is $4.72 \times 10^5 \text{ erg/cc}$. [2] With increasing t_{Pt} , K_1 decreases rapidly, passing through zero at $t_{\text{Pt}} \approx 1.8 \text{ \AA}$, which is where the easy axis switches from the bct[100] to the bct[1 $\bar{1}$ 0] direction in the multilayer. K_1 levels off around $-3.5 \times 10^5 \text{ erg/cc}$ near $t_{\text{Pt}} = 2 \text{ \AA}$ (about 1ML), beyond which its magnitude slowly increases with increasing thickness, except in the region of the crystalline phase transition (unshaded white region) where the magnitude of K_1 is slightly reduced.

It is somewhat surprising that the crystalline phase transition has so little influence on the magnetocrystalline anisotropy. By comparison, it is clear that the Fe/Pt interface plays a dominant role in the anisotropy. For Fe/TM multilayers such as these, we typically find that the interface is about 2 ML wide (see e.g. refs. [24,25]). Assuming this is true here, the interface would contain 1 ML Pt and 1 ML Fe, and would therefore be fully established for $t_{\text{Pt}} \approx 2 \text{ \AA}$. This is exactly the thickness at which K_1 stops changing.

V. X-RAY MAGNETIC CIRCULAR DICHROISM EXPERIMENTS

The Fe and Pt moments were found using x-ray magnetic circular dichroism. [4,5] These measurements are

done at the N-edge of Pt and the L-edge of Fe using the 6M and 10M TGM beamlines of the Synchrotron Radiation Center, Stoughton, WI.

By accepting x-rays emitted slightly above the horizontal plane of the bending magnet, 85% circularly polarized x-radiation is obtained. This radiation is incident at an angle of 45° upon the sample, and the plane of incidence was parallel to the applied magnetic field. An electromagnet switched the magnetization direction by 180° at each photon energy, with measurements taken in a saturated state. The total electron yield of each sample was normalized to the yield from a Cu or Ni mesh, resulting in x-ray absorption spectra. The difference in the x-ray absorption spectrum for the two magnetization directions is the XMCD.

Typical absorption and dichroism (difference) spectra for Fe and Pt are shown in fig. 6 and 7, respectively. In order to deduce the Fe and Pt moments from the dichroism signal, a method has been developed to compare the spectra from all “unknown” samples to the spectra of a “standard” sample. [17,19] For Fe, the standard was taken from a region of the multilayer sample where only Fe was deposited. The moment at this point is taken to be that of bulk Fe, $2.15 \mu_B$.

As a Pt standard, a position on the Co_xPt_y alloy film was measured where the composition is CoPt_3 . It is known that a chemically ordered phase of CoPt_3 exists with a Cu_3Au structure. One distinguishing characteristic of chemically-ordered and disordered CoPt_3 is the Curie temperature T_c (50°C and 190°C , respectively). The growth conditions under which this sample was prepared were analogous to those of a previous study which resulted in chemically-disordered alloys. [27] In line with this, the present sample shows a magnetization and remanence (as measured by MOKE) indicative of a Curie temperature T_c well above room temperature. Based on previous neutron [26] and bulk magnetometry [27] studies, it can be derived that disordered CoPt_3 has magnetic moments of 0.78 and $0.27 \mu_B$ per atom for Co and Pt, respectively. This information is used in the calibration of the Pt magnetic moments.

As a secondary calibration, we compare the Pt XMCD spectrum (fig. 7) with that in a previous XMCD study [28] of chemically-ordered CoPt_3 at the Pt N-edge. The present calibration is consistent with those results.

The XMCD-determined magnetic moments contain several sources of error. One is simple noise in the XMCD spectra, and this error can be estimated from the comparison between the sample and standard spectra. This error is only a few percent for the Fe moments, but is $\approx 20\%$ for the Pt moments. Another error comes from the reproducibility of the setting of the circular polarization shutter, which leads to variations in the magnetic moments of $\approx 10\%$. These are statistical errors, and lead to scatter in the moment data.

A third source of error comes from the assumed proportionality between the XMCD and magnetic moment. This systematic error has been discussed previously

[18,17]. Another systematic error, important only for the Pt moments, comes from the standard sample. The errors inherent in the original neutron and bulk magnetometry measurements of disordered CoPt_3 are reflected in the scaling of the Pt moments. These systematic errors may amount to 30% of the moment determination. Note that the systematic errors affect mainly the moment scales, and do not affect the general trends of the moment curves.

VI. ELEMENT SPECIFIC MAGNETOMETRY

The Fe and Pt magnetic moments (per atom) as determined by XMCD are displayed in figs. 8 and 9. For thin Pt layers (less than $\approx 4 \text{ \AA}$), the Fe XMCD is enhanced by $\approx 10\%$ over the bulk value. This enhancement is similar to (but smaller than) that observed in Fe/Rh(001) multilayers. It is also interesting to note that this enhancement of the Fe XMCD is mirrored in Θ_K^{sat} (fig. 4), which shows a 30% enhancement of the Kerr effect over the same thickness range.

However, we must take care in drawing conclusions about the Fe moment because of the systematic errors inherent in XMCD. The orbital moment and magnetic dipole contributions to the XMCD signal are expected to vary most strongly over the thickness range where the bulk 3-D symmetry of the Fe is first broken by the Pt layers, that is, during the establishment of the Fe/Pt interface.

Comparing with previous results, another dichroism study discussing Fe/Pt fct(111) multilayers showed a similar enhancement. Another report of bulk magnetometry from Fe/Pt(001) [3] showed no evidence for enhancement of the Fe moment. However, in the latter case the Fe layers were much thicker than here, which would dilute any enhancement rendering it immeasurable. Thus with the present data we must consider the assignment of an Fe moment enhancement as tentative.

There is a sharp, 20% decrease of the Fe moment in the region of the bct \rightarrow fct phase transition (unshaded region in fig. 8). Although this drop occurs in a region where the Fe symmetry is rapidly changing, it is large enough to indicate some change in the Fe magnetic moment. A small drop in the Fe moment associated with phase change also appears in bulk magnetometry measurements [3]. However, note once again that the latter study employed thicker Fe layers, which probably accounts for the discrepancy in the magnitude of the Fe moment change.

Fig. 9 shows the measured Pt moments as a function of Pt thickness (error bars represent only the statistical errors). The Pt moment per atom is constant at $\approx 0.5 \mu_B$ with increasing Pt thickness. This is quite surprising since in most other Fe/TM multilayers, the TM atomic moment decays exponentially toward the center of the layer (see e.g. Refs. [17,24,21]). To our knowledge, the

only other system which displays such “almost ferromagnetic” behavior is Fe/Rh(001) where the Rh moment is stable (at $\approx 1\mu_B$) for as long as the multilayer remains bct. The present case is even more striking since the phase transition has no observable effect on the Pt moment, which remains constant up to at least $t_{\text{Pt}} = 10 \text{ \AA}$ (5 ML). This result is entirely new, since no previous study of Fe/Pt multilayers has considered the Pt moments.

The one point that deviates most from the straight line in fig. 9 is the first, with $t_{\text{Pt}} = 0.9 \text{ \AA}$. At this submonolayer thickness, the film might be represented as Fe₇₀Pt₃₀ alloy layers separated by Fe layers (assuming 2 ML of interdiffusion at each interface). In this alloy regime, the induced Pt moment is comparable to that in bulk Fe₃Pt alloys where the induced Pt moment is $0.36\mu_B$. [22] For larger t_{Pt} , the effective concentration of Pt goes up, and the induced Pt moment might be expected to decrease. In contrast, we observe that the Pt moment *increases* with increasing t_{Pt} . Furthermore, these observed Pt moments are well above those in alloys with the same average concentration. We have seen this kind of behavior before in e.g. Fe/Cr [17], Fe/Rh [19], Fe/V [24], and elsewhere. It seems an almost generic property that the induced moments in nonmagnetic elements are larger in multilayers than in bulk random alloys.

Finally, we point out the near constant Pt moment in the fct region is accompanied by a gradual decay of the Fe moment. By comparison, bulk magnetometry showed no measurable change of the magnetization over this thickness range [3]. Yet the present data are in agreement with the previous study because bulk magnetometry measures the sum of the Fe and Pt magnetic moments. For example, a weighted sum of the Fe and Pt moments at $t_{\text{Pt}} = 10 \text{ \AA}$ leads to a net moment of $\approx 2.1\mu_B$ per iron atom, in good agreement with Ref. [3]. This points out the importance of performing element-specific magnetometry, since without it one would naturally assume that the Pt had negligible magnetic moment while the Fe moment was unchanged.

VII. DISCUSSION

It is notable that the fct Fe remains ferromagnetic for the entire range of Pt thicknesses studied. Similar results were previously reported for Fe/Pt using bulk magnetometry, [2] and Fe/Pd multilayers display a similar behavior. In contrast to this, some other nonmagnetic fcc transition metals (e.g. Cu, Rh) result in fct Fe/TM multilayers that are paramagnetic at room temperature. [23,19] Similarly, we note that Fe/Ru multilayers transform to the hcp structure (another close-packed phase) and also result in a paramagnetic material. [21] The different behavior of Pt and Pd in multilayers might be ascribed to the fact that Pt and Pd have relatively large LC’s. It is well known [30] that the magnetic state of close-packed Fe depends critically on the LC, and that a larger LC

favors the ferromagnetic state. For even larger fcc LC (e.g. Ag, Au) the Fe also remains magnetic but is in a bcc phase, rotated by 45° with respect to the TM lattice.

The induced magnetism within the Pt layers is so strong, that it may well be regarded as in a ferromagnetic state. Of course, this ferromagnetism is supported by the magnetic Fe at the interface, but the Pt layers are thick enough that we can safely assume that Pt atoms with no Fe nearest neighbors nevertheless possess a magnetic moment. This gives us a unique opportunity to study the “bulk” magnetic properties of a new ferromagnetic element.

For example, we can say something about the volume anisotropy constant for ferromagnetic Pt. Returning to fig. 5, we see that for $t_{\text{Pt}} = 4.5\text{--}8 \text{ \AA}$, the anisotropy constant is gradually increasing in magnitude. This suggests that the volume anisotropy constant of ferromagnetic Pt is not negligible.

To quantify the interface and volume anisotropy contributions to K_1 , we expand it as

$$K_1 = [K_V^{\text{Fe}} + 2K_s^{\text{Fe}}/t_{\text{Fe}}] \frac{t_{\text{Fe}}m_{\text{Fe}}}{t_{\text{Fe}}m_{\text{Fe}} + t_{\text{Pt}}m_{\text{Pt}}} + [K_V^{\text{Pt}} + 2K_s^{\text{Pt}}/t_{\text{Pt}}] \frac{t_{\text{Pt}}m_{\text{Pt}}}{t_{\text{Fe}}m_{\text{Fe}} + t_{\text{Pt}}m_{\text{Pt}}}. \quad (4)$$

Here m_A is the experimentally determined magnetic moment per atom of element A. Note that since t_{Fe} is held constant in the present study, K_s^{Pt} cannot be determined independently from K_s^{Fe} . In this case it is sufficient to assume (as is usually done) that $K_s^{\text{Pt}} = 0$, and we do this here.

Using the experimental anisotropy value from $t_{\text{Pt}} = 0$, we can use this equation to determine $K_V^{\text{Fe}} = 5.4 \times 10^5$ erg/cc. This is close to that of bulk Fe, and the slight deviation may be attributed to the in plane tensile strain of the Fe grown on MgO(001). To determine K_s^{Fe} we use the experimental anisotropy at $t_{\text{Pt}} = 2 \text{ \AA}$ where the Fe/Pt interface has just been established. We determine a value of $K_s^{\text{Fe}} = -0.029$ erg/cm² which is the same as found in Ref. [2], in spite of the fact that the previous study employed much thicker Fe and Pt layers.

Lastly, equation 4 may be fit to the anisotropy data beyond $t_{\text{Pt}} = 2 \text{ \AA}$ to estimate K_V^{Pt} . Using this procedure we find $K_V^{\text{Pt}} = -8 \pm 2 \times 10^5$ erg/cc. The best fit to the anisotropy data is plotted as a solid line in fig. 5, while another fit assuming $K_V^{\text{Pt}} = 0$ is plotted as a dashed line. The solid line shows better agreement with the data. This interpretation and the value of K_V^{Pt} is plausible, but note that we have ignored magnetoelastic contributions to the anisotropy which could also play an important role. Still, we argue that Pt contributions to the anisotropy need not be small.

Specifically, consider the Pt surface anisotropy constant K_s^{Pt} . Historically, the surface anisotropy has been attributed only to atoms at the surface of the ferromagnetic layer. But it is quite likely that magnetized Pt interface atoms contribute strongly to the surface anisotropy

here. Pt has a spin-orbit coupling that is eight times larger than that in Fe, while the Pt moment here is about one quarter as large as Fe. Because the anisotropy depends linearly on the orbital moment, which scales linearly with the spin-orbit coupling [13], we can estimate that two thirds of the surface anisotropy arises from the Pt interface atoms, while only one third comes from the interface Fe. Although the present Pt XMCD data do not support an orbital moment analysis, perhaps future studies at the Pt L-edge could directly measure the interfacial Pt orbital moments and test this hypothesis.

From this study we arrive at several conclusions. Firstly, the Pt atoms acquire a significant magnetic moment in Fe/Pt multilayers. This moment must be included in any interpretation of bulk magnetometry data. For example, we have seen that for $t_{\text{Pt}} > 4 \text{ \AA}$, the Fe moment is depressed. But the nonzero Pt moment gives the illusion that the Fe moment is unchanged. Similarly, any measurement of the magnetic anisotropy of such multilayers should include the Pt moment *and* Pt contributions to the volume and surface anisotropy.

VIII. CONCLUSION

The (001) Fe/Pt multilayer system is investigated as a function of Pt thickness. We have shown that the multilayer's crystal structure switches from bct to fct as the Pt thickness is increased. The Fe moment and Kerr response are both suppressed upon phase change. Unlike some other Fe/fcc TM systems the fct Fe is found to remain ferromagnetic. A nearly constant Pt moment of $\approx 0.5 \mu_B$ is observed for $0 < t_{\text{Pt}} < 10 \text{ \AA}$. Finally, the first anisotropy constant K_1 is found using two independent methods, and it has a zero crossing near $t_{\text{Pt}} = 1.8 \text{ \AA}$. Changes in the anisotropy are found to occur independently of the crystal structure change. We conclude that both the moment and anisotropy of Pt contribute significantly to the measured value of K_1 .

The authors gratefully acknowledge Prof. B. Heinrich for helpful discussions. The authors acknowledge support of the National Science Foundation CAREER Award No. DMR-9623246. The Synchrotron Radiation Center is supported by the NSF under Award No. DMR-9531009.

-
- [1] See e.g. A. Simopoulos, E. Devlin, A. Kostikas, Alan Jankowski, Mark Croft, and Thomas Tsakalakos, Phys. Rev. B **54**, 14 9931 (1996) and references therein.
 [2] M. Sakurai, Phys. Rev. B **50**, 6 3761 (1994).
 [3] M. Sakurai, N. Imamura, K. Hirano, and T. Shinjo, J. Magn. Magn. Mater. **147**, 16 (1995).

- [4] J.L. Erskine and E.A. Stern, Phys. Rev. B **12**, 5016 (1975).
 [5] G. Schütz, W. Wagner, P. Keinle, R. Zeller, R. Frahm, and G. Materlik, Phys. Rev. Lett. **58**, 737 (1987).
 [6] J. E. Mattson, E. E. Fullerton, C. H. Sowers, and S. D. Bader, J Vac. Sci. Tech. **13**, 2 276 (1995).
 [7] G. R. Harp and S. S. P. Parkin, Appl. Phys. Lett. **65**, 3063 (1994).
 [8] B. E. Warren, *X-ray Diffraction*, New York: Dover Publications, 1990, pg. 253.
 [9] P. Isberg, B. Hjörvarsson, R. Wäppling, E. B. Svedberg, and L. Hultman, Vacuum, **48**, 483 (1997).
 [10] E. Devlin, V. Psycharis, A. Kostikas, A. Simopoulos, D. Niarchos, A. Jankowski, T. Tsakalakos, Hong Wan, and G. Hadjipanayis, J. Magn. Magn. Mater. **120**, 236 1993.
 [11] T. Katayama, Y. Suzuki, Y. Nishihara, T. Sugimoto and M. Hashimoto, J. Appl. Phys. **69**, 5658 (1991).
 [12] P. Bruno, *Magnetismus von Festkörpern und Grenzflächen*, Ferienkurse des Forschungszentrums, kFA, Jülich, ISBN 3-89336-110-3, 24.1-24.27 (1993).
 [13] D. K. Misemer, J. Magn. Magn. Mater. **72**, 267 (1988).
 [14] F. Brailsford *Physical Principles of Magnetism*, New York: Van Norstrand (1966).
 [15] Note that the interpretation of K_1 depends on whether one indexes the lattice using a bct or fct system. In going from the bct to fct lattice, one effectively interchanges the meaning of the [100] and [110] directions, which reverses the sign of K_1 . To minimize confusion, here we use a consistent bct indexing throughout the discussion of the anisotropy.
 [16] M. A. Tomaz, W. J. Antel Jr., W. L. O'Brien, and G. R. Harp, Phys. Rev. B **55**, 3716 (1997).
 [17] D. Weller, J. Stöhr, R. Nakajima, A. Carl, M. G. Samant, C. Chappert, R. Megy, P. Beauvillian, F. Veillet, and G. Held, Phys. Rev. Lett. **75**, 3752 (1995).
 [18] M. A. Tomaz, D. C. Ingram, G. R. Harp, D. Lederman, E. Mayo, and W. L. O'Brien, Phys. Rev. B **56**, 5474 (1997).
 [19] Tao Lin, M. M. Schwickert, M. A. Tomaz, H. Chen, and G. R. Harp, submitted to Phys. Rev. B.
 [20] Tao Lin, M. A. Tomaz, M. M. Schwickert, and G. R. Harp, Phys. Rev. B **58**, 862 (1998).
 [21] K. Adachi, in *3d, 4d, and 5d Elements, Alloys, and Compounds*, edited by H. P. J. Wijn, Landolt-Börnstein, New Series, Group 3, Vol. 19a, p. 597 (Springer Verlag, Berlin, 1986).
 [22] See e.g. D. Li, J. Pearson, Z. Q. Qiu, and S. D. Bader, Phys. Rev. Lett. **72**, 3112 (1994).
 [23] M. M. Schwickert, R. Coehoorn, M. A. Tomaz, E. Mayo, D. Lederman, W. L. O'Brien, Tao Lin and G. R. Harp, Phys. Rev. B **57**, 13681 (1998).
 [24] M. A. Tomaz, G. R. Harp, E. Mayo, D. Lederman R. Wu, and W. L. O'Brien, J. Vac. Sci. Technol. A **16**, 1336 (1998).
 [25] F. Menzinger and A. Paoletti, Phys. Rev. **143**, 365 (1966).
 [26] D. Weller, R. F. C. Farrow, J. E. Hurst, H. Notarys, H. Brändle, M. Rührig, and A. Hubert, Optical Memory and Neural Networks **3**, 353 (1994).
 [27] T. Shishidou, S. Imada, T. Muro, F. Oda, A. Kimura, S.

Suga, T. Miyahara, T. Kanomata, and T. Kaneko, Phys. Rev. B **55**, 6 3749 (1997).

- [28] M. A. Tomaz, W. J. Antel Jr, W. L. O'Brien, and G. R. Harp, J. Phys.: Condens. Matter **9**, L179-L184 (1997).
 [29] V. L. Moruzzi, P. M. Marcus, K. Schwarz and P. Mohn, Phys. Rev. B **34**, 1784 (1986).
 [30] G. R. Harp, et al. to be published.

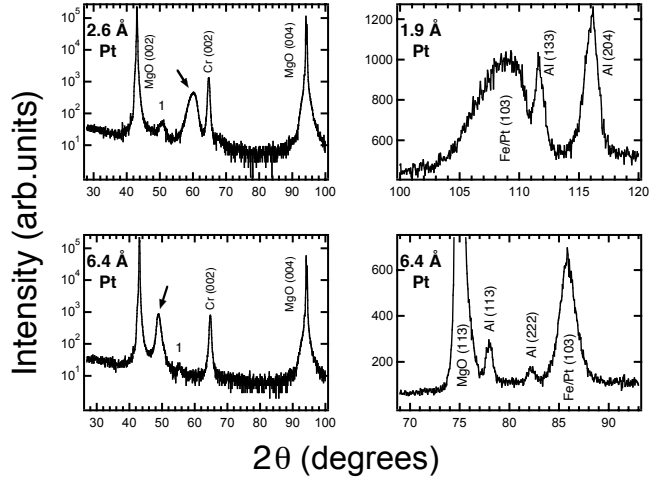


FIG. 1. X-ray diffraction c -axis radial scans (left) and off-normal radial scans (right) for various Pt thicknesses, as indicated. For the c -axis scans, the Fe/Pt(002) peak is marked with an arrow, and multilayer satellites of this peak are also visible. No other Fe/Pt related features are present, indicating a single (001) orientation for these films. The off-normal scans are through the Fe/Pt bct(103) feature. Several Al features are present due to the sample holder. From these scans we determine in plane lattice constants for these films.

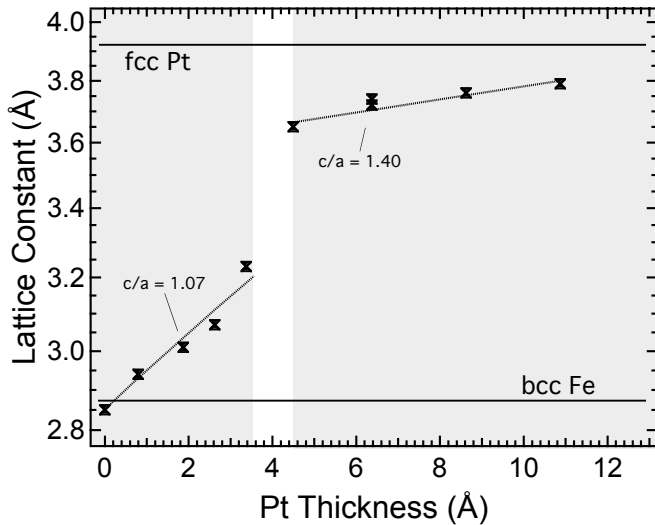


FIG. 2. Plot of c -axis average Fe/Pt lattice constant vs. Pt thickness. The symbols are the data extracted from c -axis radial scans, the dotted lines are guides to the eye. The jump and change in slope for $t_{Pt} \approx 4$ Å indicates a crystalline phase transition from bct to fct for the Fe/Pt multilayer. c/a ratios, indexed on a bct lattice, are indicated for two points on the figure. Recall that the perfect bcc (fcc) lattice should have a c/a ratio of 1.00 (1.41). The unshaded vertical stripe in the figure indicates the region of the phase transition.

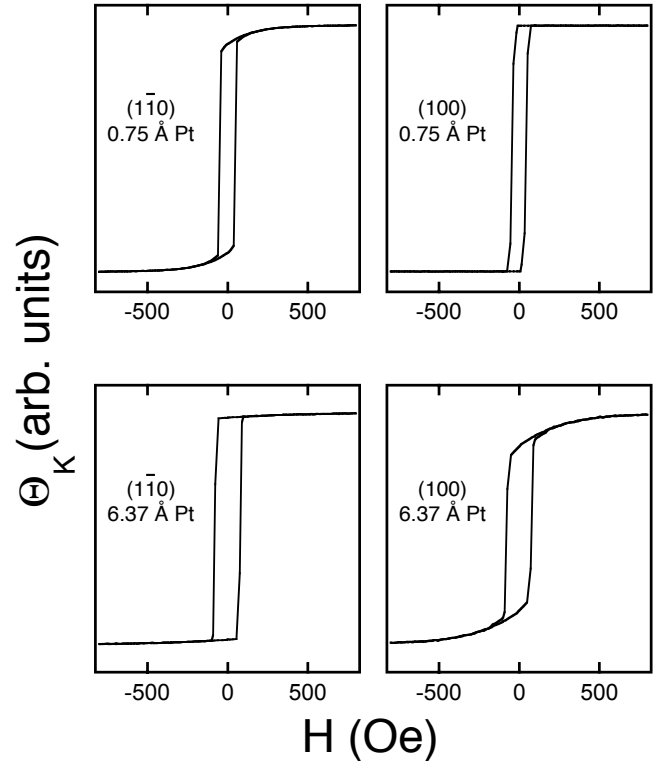


FIG. 3. In plane MOKE loops for two Pt thicknesses along bct[100] and bct[$1\bar{1}0$] directions. From loops such as these, the saturation Kerr effect and in plane magnetic anisotropy are determined. It is observed that the easy axis switches from the [100] to the [$1\bar{1}0$] direction with increasing t_{Pt} .

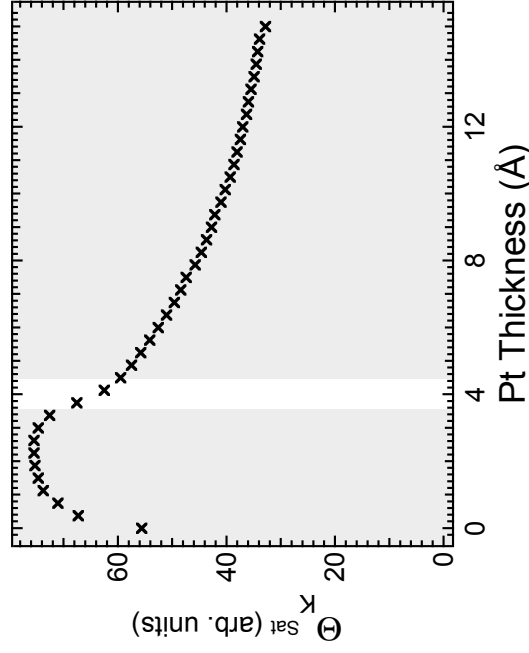


FIG. 4. The saturation Kerr effect Θ_K^{Sat} as a function of Pt thickness. There is a strong enhancement of the Kerr effect for thin Pt layers, followed by a sharp downturn as the film transforms from bct to fct (unshaded white region). Following the phase transition, the Kerr effect decreases smoothly, as expected from a simple dilution of the Kerr effect with the addition of Pt.

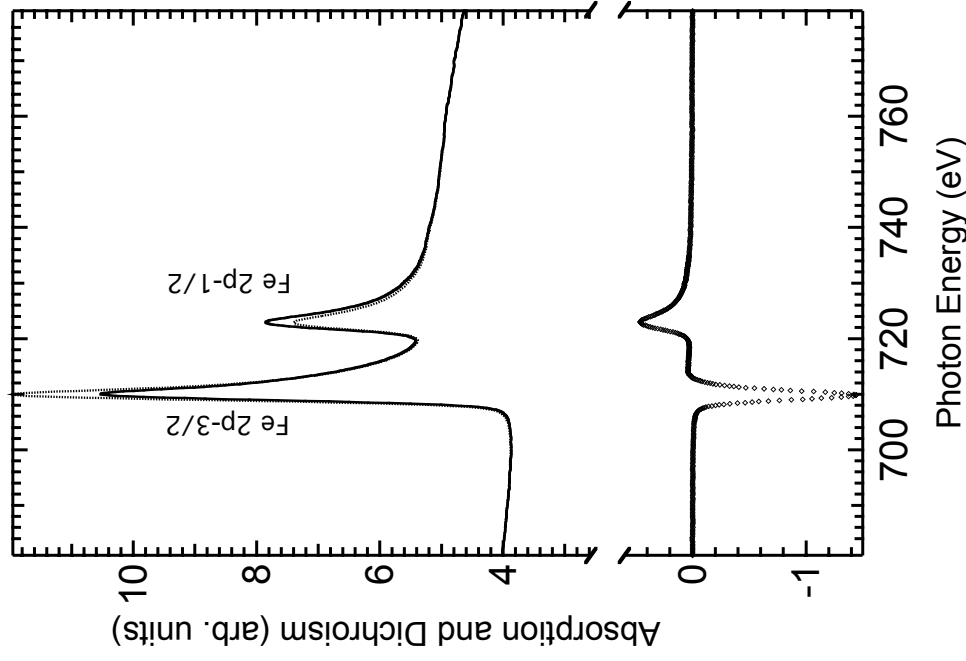


FIG. 6. Fe $L_{2,3}$ absorption (solid and dashed line) and dichroism (symbols) at a position in the Fe/Pt multilayer with $t_{\text{Pt}}=6.8$ Å. From these data we deduce an Fe magnetic moment of $1.86\mu_B$.

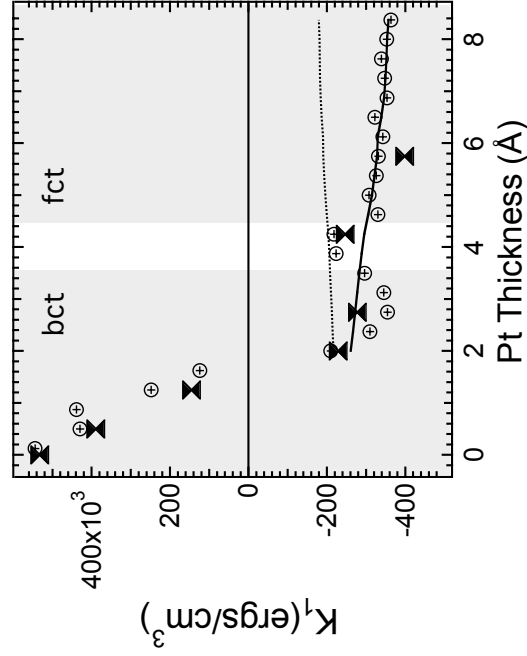


FIG. 5. In plane magnetocrystalline anisotropy constant, K_1 , as a function of Pt thickness. Results are shown for K_1 as determined by two methods: (circled crosses) from the saturation field along the hard axis and (bowties) from the 95% saturation field as a function of in plane direction, as discussed in the text. The greatest variation of anisotropy constant occurs with the creation of the Fe/Pt interface. Once the interface is fully established (≈ 2 Å Pt), there is little change in K_1 with increasing t_{Pt} apart from a blip in the region of the crystalline phase transition (unshaded white region). The solid and dashed lines are fits to the data discussed in the text.

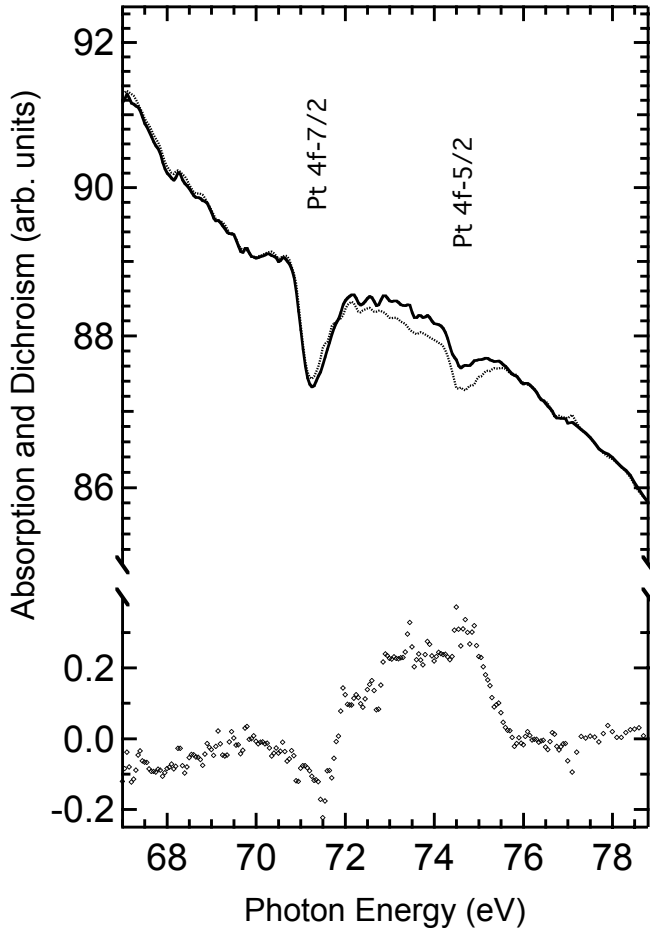


FIG. 7. Pt $N_{2,3}$ absorption (solid and dashed line) and dichroism (symbols) from the Fe/Pt multilayer with $t_{Pt} = 6.8 \text{ \AA}$. The absorption edges have a Fano line shape which has been observed in previous studies. The dichroism is similar in shape to that observed elsewhere, and indicates a Pt magnetic moment of $\approx 0.5 \mu_B$ for this film.

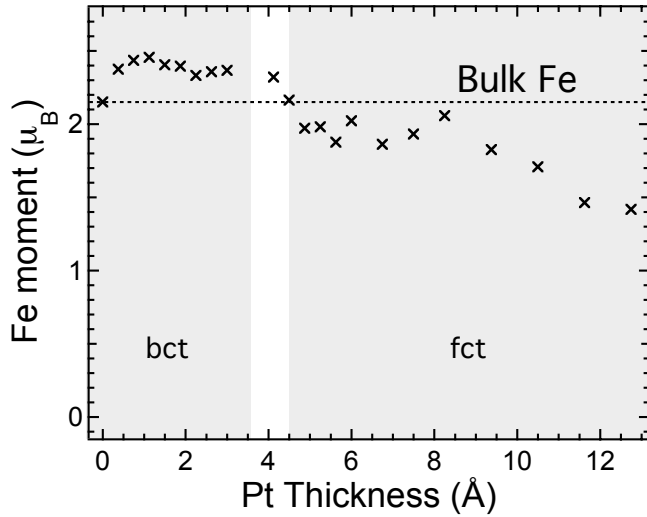


FIG. 8. Average Fe moment per atom vs. Pt thickness as determined by XMCD. For thin Pt layers there is an enhancement in the Fe XMCD over the bulk bcc value. Upon phase transition to fct (unshaded white region) the Fe moment drops significantly. Thereafter the fct Fe remains ferromagnetic throughout the Pt thickness range studied.

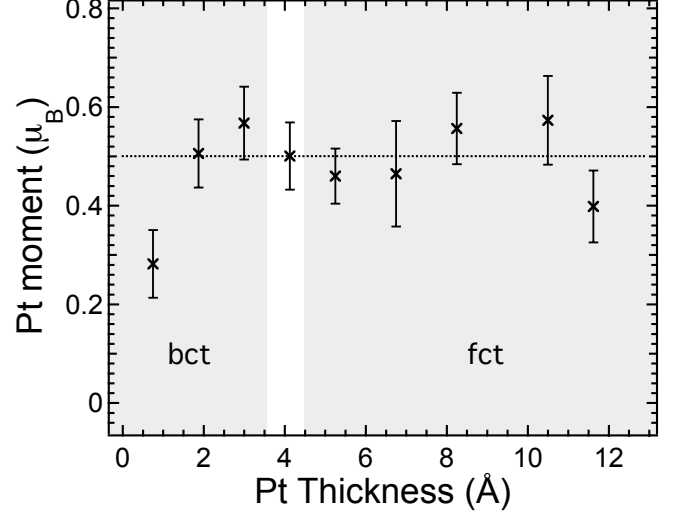


FIG. 9. Average Pt moment per atom vs. Pt thickness, as determined by XMCD. The moment is almost constant at a value of $\approx 0.5 \mu_B$ (dotted line) over the entire Pt thickness range. This implies that the Pt is ferromagnetic throughout the entire layer and not just at the interface with Fe.